

## Quantum Spin Hall States and Topological Phase Transition in Germanene

Pantelis Bampoulis<sup>1,\*</sup>, Carolien Castenmiller<sup>1</sup>, Dennis J. Klaassen<sup>1</sup>, Jelle van Mil,<sup>1</sup>  
Yichen Liu,<sup>2</sup> Cheng-Cheng Liu<sup>2</sup>, Yugui Yao,<sup>2</sup> Motohiko Ezawa,<sup>3</sup>  
Alexander N. Rudenko<sup>4</sup>, and Harold J. W. Zandvliet<sup>1</sup>

<sup>1</sup>*Physics of Interfaces and Nanomaterials, MESA+ Institute, University of Twente,  
Drienerlolaan 5, 7522 NB, Enschede, Netherlands*

<sup>2</sup>*Centre for Quantum Physics, Key Laboratory of Advanced Optoelectronic Quantum Architecture and Measurement (MOE),  
School of Physics, Beijing Institute of Technology, Beijing 100081, China*

<sup>3</sup>*Department of Applied Physics, University of Tokyo, Hongo, 113-8656 Tokyo, Japan*

<sup>4</sup>*Institute for Molecules and Materials, Radboud University Nijmegen, Heyendaalseweg 135,  
6525 AJ Nijmegen, Netherlands*



(Received 9 November 2022; accepted 24 March 2023; published 12 May 2023)

We present the first experimental evidence of a topological phase transition in a monoelemental quantum spin Hall insulator. Particularly, we show that low-buckled epitaxial germanene is a quantum spin Hall insulator with a large bulk gap and robust metallic edges. Applying a critical perpendicular electric field closes the topological gap and makes germanene a Dirac semimetal. Increasing the electric field further results in the opening of a trivial gap and disappearance of the metallic edge states. This electric field-induced switching of the topological state and the sizable gap make germanene suitable for room-temperature topological field-effect transistors, which could revolutionize low-energy electronics.

DOI: 10.1103/PhysRevLett.130.196401

The realization of the topological field-effect transistor requires an electric field-induced transition from a quantum spin Hall (QSH) insulator with dissipationless conductive channels (*on*) to a trivial insulator (*off*). QSH insulators have an energy gap in their bulk and two topologically protected gapless helical edge states. Kane and Mele [1,2] derived the QSH effect in graphene based on Haldane's proposed topological state [3] and taking into account spin-orbit coupling (SOC). The SOC results in an internal magnetic field pushing spin-up and spin-down electrons in opposite directions toward the edges of the material, see illustration in Fig. 1(a). Time-reversal symmetry and spin-orbit interaction lead to spin-momentum locking, prohibiting backscattering from nonmagnetic impurities and allowing for dissipationless electronic transport along the material's edges [1,4–8].

The first realizations of the QSH effect were not for graphene, but for band inverted semiconductors and 2D materials [9–16], following the Bernevig-Hughes-Zhang model [5]. The QSH (monoelemental) honeycomb material described by the Kane-Mele model [1,2] has yet to be experimentally discovered. Graphene has very small SOC [17], requiring very low temperatures to investigate the QSH effect. Since SOC depends on the atomic number ( $\sim Z^4$ ), graphenelike materials made out of heavier elements have recently been synthesized and scrutinized [18–26]. One of these materials is germanene, the germanium analog of graphene [18]. The predicted SOC gap for germanene is 23.9 meV [27], large enough to exhibit the QSH effect

at experimentally accessible temperatures. In addition, germanene has a buckled honeycomb lattice [28], see Fig. 1(a). The buckling separates the inverted orbitals of germanene across different atomic planes, offering the possibility to alter the topological state of germanene by the application of an external electric field, perpendicular to the layer [16,29–33].

We have employed low-temperature scanning tunneling microscopy (STM) and spectroscopy (STS), density functional theory (DFT), and tight-binding (TB) calculations to demonstrate that epitaxial germanene on  $\text{Ge}_2\text{Pt}(101)$  is a buckled-honeycomb QSH insulator. At its QSH state, germanene is characterized by a bulk gap and metallic nontrivial edge states. We controlled the built-in electric field in the tip-sample tunneling junction to alter the topological state of germanene. At a critical electric field, germanene's topological gap closes. The material transforms into a topological semimetal. Above the critical field, a trivial band gap opens accompanied by the disappearance of the edge states.

Germanene is grown on  $\text{Ge}_2\text{Pt}(101)$  following the procedure in Ref. [20], for details see Supplemental Material (SM) [34]. A large-scale STM topograph of few-layer germanene on  $\text{Ge}_2\text{Pt}(101)$  is shown in Fig. 1(b), the number of layers is indicated in the image. The first layer of germanium on  $\text{Ge}_2\text{Pt}(101)$  has a (distorted) honeycomb structure. This layer acts as a buffer layer and electronically decouples the next germanene layer from the substrate, see SM and Fig. S1 for details. The rest of the

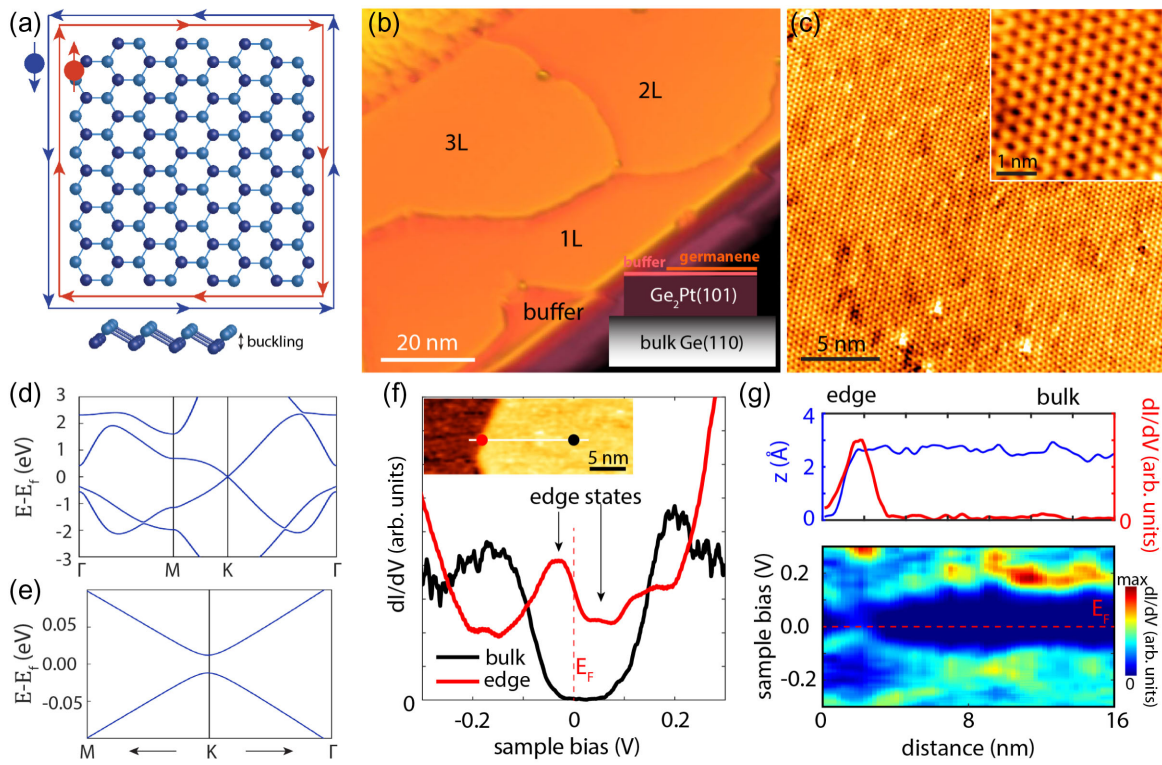


FIG. 1. (a) Schematic of the QSH effect in the buckled honeycomb of germanene (the bottom image is a side view). (b) STM image of few-layer germanene on  $\text{Ge}_2\text{Pt}(101)$ , the number of layers is indicated. Inset: cartoon of the system. (c) Large-scale STM image of the honeycomb lattice of the first decoupled germanene layer, with a close-up view in the inset. (d) DFT calculations of the band structure of freestanding germanene with SOC. (e) Close-up of (d) around the  $K$  point to show the SOC gap of germanene. (f)  $dI(V)/dV$  spectra recorded at the bulk and edge of germanene, indicated with black and red dots in the topography shown in the inset. (g) (Bottom) a  $dI(V)/dV$  line spectroscopy recorded as a function of distance across the germanene edge [indicated with the white solid line in the topography in panel (f)]. (Top) The topography cross section (blue) and  $dI/dV$  cross section at  $E_F$  (red) of the line spectroscopy (bottom).

manuscript focuses on the first decoupled monolayer, i.e., germanene on the buffer layer on  $\text{Ge}_2\text{Pt}$ , hereafter referred to as germanene. Figure 1(c) and its inset provide close-up images of germanene, revealing its buckled honeycomb lattice. We extract a lattice constant of  $(0.43 \pm 0.02)$  nm, a monoatomic step height of  $(0.28 \pm 0.02)$  nm and a buckling of  $\sim 0.03\text{--}0.04$  nm. Without SOC, germanene is a semimetal, characterized by linear energy bands at the  $K$  and  $K'$  (Dirac) points of the Brillouin zone [32]. However, SOC opens up a small topological gap in germanene. As shown in our first-principle calculations in Figs. 1(d) and 1(e), the topological gap of freestanding germanene is 23.9 meV, in agreement with Ref. [27]. Therefore, germanene is expected to be a QSH insulator, characterized by a bulk band gap and topologically protected metallic edge states [18,32].

The first evidence on the QSH state of germanene comes from spatially resolved DOS measurements done with STS. Figure 1(f) shows local differential conductance [ $dI(V)/dV$ ] spectra recorded at the edge (red) and bulk (black,  $\sim 15$  nm away from the edge) of germanene, the locations are indicated with red and black circles in the inset. The  $dI(V)/dV$  spectrum of the bulk reveals a band

gap of  $\sim 70$  meV. Similar spectra have been observed on several different samples, with minor differences in gap size and doping. For additional spectra and details on the determination of the gap, see SM and Fig. S2 [34]. The size of the gap is larger than the DFT predictions for freestanding germanene. This discrepancy cannot be explained by strain or buckling, see Fig. S3. The actual cause might be a complicated interplay between strain, buckling, stacking (germanene/buffer/ $\text{Ge}_2\text{Pt}$ ) and proximity effects. Stacking has been shown to increase the topological gap of germanene up to 100 meV [55,56], and proximity effects have been reported to lead to significant increase of topological gaps [57,58]. Our DFT calculations, Fig. S4, show that indeed the Pt-Ge distance impacts the topological gap; the gap exceeds 100 meV at short Pt-Ge distances and approaches the freestanding value for longer distances. Below 3 Å, the linear dispersion close to the  $K$  point is destroyed by the hybridization between Ge and Pt, which is in agreement with our STS data on the buffer layer, Fig. S1f in SM [34]. However, a comprehensive understanding of the large band gap of germanene requires a more rigorous approach and consideration of stacking order, strain, buckling, and proximity effects.

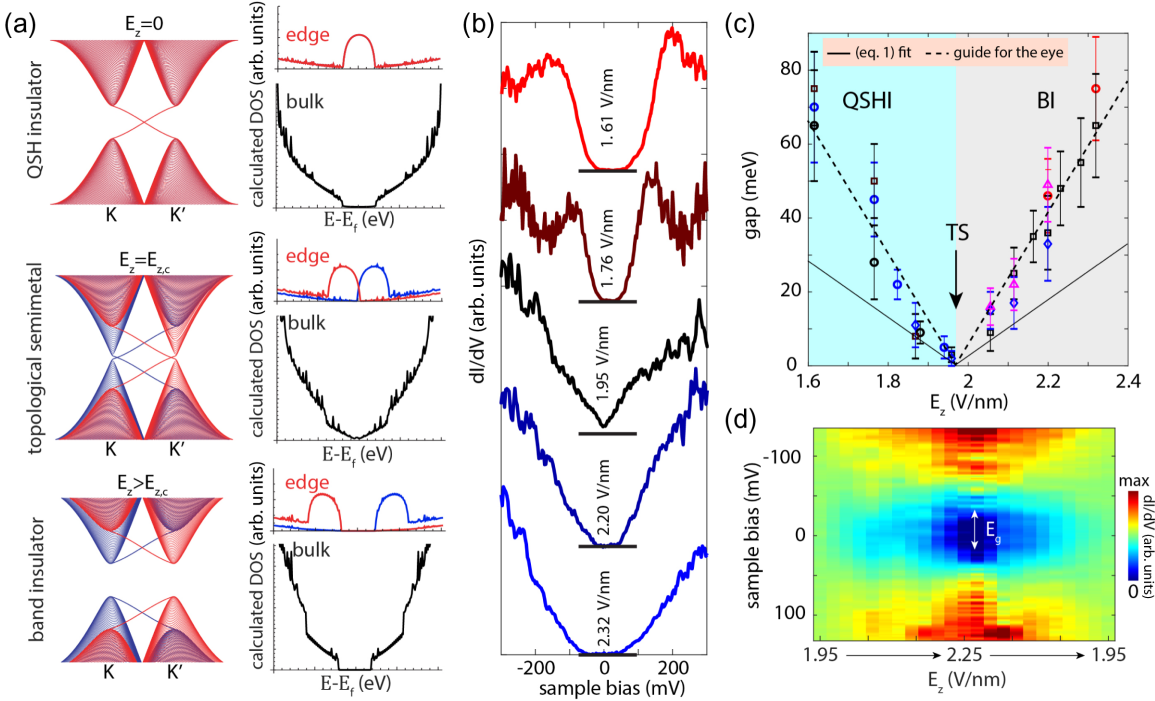


FIG. 2. (a) TB calculations of the band structure (left) at the  $K$  and  $K'$  points of the Brillouin zone, and DOS of the bulk and edges (right) of germanene under the influence of perpendicular electric fields; (top)  $E_z = 0$ , (middle)  $E_z = E_{z,c}$ , (bottom)  $E_z > E_{z,c}$ . Red and blue bands correspond, respectively, to spin-up and spin-down electrons. For  $E_z = 0$  the bands overlap. (b)  $dI(V)/dV$  spectra for five different electric fields:  $\sim 1.61$  V/nm,  $\sim 1.76$  V/nm,  $\sim 1.95$  V/nm,  $\sim 2.20$  V/nm,  $\sim 2.32$  V/nm. The spectra are vertically offset for clarity and the zero  $dI/dV$  levels are indicated with black lines. (c) Band gap size as a function of the electric field. The material transitions from a QSH insulator to a topological semimetal (TS) and finally to a trivial band insulator (BI). The black line is a fit to the data using Eq. (1), and the dashed black line is a guide for the eye. The different markers indicate experiments done on different samples. (d)  $dI(V, E_z)/dV$  map showing the opening of a trivial gap with increasing the electric field from 1.95 to 2.25 V/nm and the closing of the gap upon reduction back to 1.95 V/nm.

In contrast to the bulk gap, the  $dI(V)/dV$  spectrum at a germanene edge, Fig. 1(f), exhibits a metallic character with enhanced DOS and pronounced electronic states. Figure 1(g) shows  $dI(V)/dV$  line spectroscopy (bottom) recorded across a monoatomic step in germanene [the location is marked with a white line in the inset of Fig. 1(f)], showing localization of the metallic states at the germanene edge (the states decay within 3–4 nm to the bulk). The top panel of Fig. 1(g) shows the corresponding topography cross section across the step, and the  $dI/dV$  cross section at the Fermi level ( $E_F$ ), demonstrating a large increase of the DOS at the edge. The edge states run uninterrupted along the edges of germanene with minor intensity variations, see  $dI/dV$  mapping as a function of the energy in Fig. S5a [34]. Moreover, the metallic edge states are robust to disorder and exist in all our samples regardless of edge termination and roughness, see Figs. S5b–S5e. These characteristics cannot be explained by trivial edge states, such as dangling bond states, zigzag states, strain. The bulk band gap and robust, termination-independent, 1D metallic edge states are signatures of a QSH insulator. Similar observations have been attributed to topology in other 2D materials, e.g., 1T'-WTe<sub>2</sub>, Na<sub>3</sub>Bi, bismuthene [14,22,59,60].

The buckling separates the inverted orbitals of germanene across different atomic planes, allowing for topological phase transitions to take place. TB calculations, Fig. 2(a), reveal that upon the application of a perpendicular electric field, inversion symmetry breaks [18,29,32,61], and charge shifts from one sublattice to the other. This leads to a closure of the topological gap at a certain critical field, and the material becomes a topological semimetal with two Dirac cones at the  $K$  and  $K'$  points of the Brillouin zone [Fig. 2(a), middle panel]. The band gap reopens for sufficiently strong electric fields but becomes topologically trivial. This is accompanied by the disappearance of the topologically protected edge channels [bottom panel of Fig. 2(a)].

To test this prediction and verify that germanene is a QSH insulator, we investigated the effect of a perpendicular electric field on the electronic band structure of germanene. We used the built-in electric field formed in the tip-sample tunnel junction. The difference in work functions between the STM tip (Au  $\sim 5.2$  eV, Pt  $\sim 5.7$  eV) and germanene ( $\sim 4$  eV [62]) generates an electrostatic potential difference, see schematic in SM Fig. S6a [34]. The strength of the electric field [ $E_z = V_s/z + (\Phi_{\text{tip}} - \Phi_{\text{germanene}})/ez$ , where  $e$  is the elementary charge] is tuned by (i) varying the

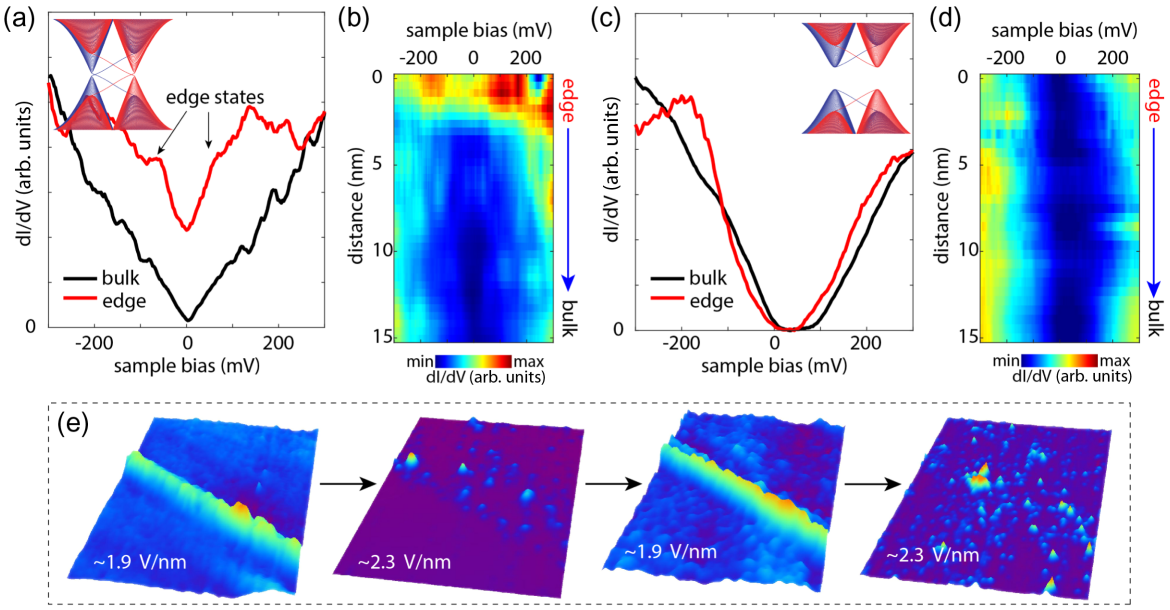


FIG. 3.  $dI(V)/dV$  point spectra recorded at the bulk and step edges of germanene for electric fields of (a)  $\sim 1.95$  V/nm and (c)  $\sim 2.32$  V/nm. (a) shows a V-shaped DOS and (c) a trivial gap. Insets: (a) topological semimetal and (c) trivial band insulator band structures. Line  $dI(V)/dV$  spectroscopy as a function of distance from the step edge (top) to the bulk of germanene (bottom) for electric fields of (b)  $\sim 1.95$  V/nm and (d)  $\sim 2.32$  V/nm, revealing the (b) presence and (d) absence of edge states. (e)  $dI/dV$  maps demonstrating the reversible *on* and *off* switching of the edge channels with the electric field.

tip-sample separation distance ( $z$ ) in a controlled manner and/or (ii) coating the STM tip with different metals, thus changing its work function ( $\Phi_{\text{tip}}$ ). Here, we have used Au and Pt coated tips to cover a large range of electric fields. The sample bias term ( $V_s$ ) is much smaller than the electrostatic potential difference and thus not taken into account. Details on preparation of the STM tips, and calculations of the electric field and tip-sample distance are given in SM.  $dI(V)/dV$  spectra recorded at the bulk of germanene for increasing perpendicular electric fields from  $\sim 1.6$  V/nm to  $\sim 2.3$  V/nm are given in Fig. 2(b), the data are offset for clarity. The topological gap of germanene is visible at  $\sim 1.6$  V/nm (at this phase the topological edge states are present, see Fig. 1). Increasing the field gradually up to  $\sim 1.95$  V/nm results in a decrease in the size of the topological gap. At the critical field,  $E_{z,c} \sim 1.95$  V/nm, the topological gap of germanene is completely closed, and the DOS has a gapless V-shaped character. At this stage, the material is a topological semimetal and in the bulk, the low-energy electrons obey the Dirac equation. Increasing the electric field further leads to the opening of a small band gap ( $\sim 70$  meV for a field of  $\sim 2.3$  V/nm). As shown in Fig. 2(a), the absence of band inversion makes this gap topologically trivial.

Figure 2(c) shows the gap size measured at various samples as a function of the applied electric field. The results are consistent with the tight-binding calculations of Fig. 2(a) for an electric field-induced topological transition in germanene. Without screening [61], the gap is  $2\ell|E_z - \eta s E_{z,c}|$  [Eq. (1)], see SM [34] or Ref. [29] for derivation

(here  $\ell$  is the buckling,  $s = \pm 1$  the spin index, and  $\eta = \pm$  the valley index). Equation (1) fits the observed trend in our data qualitatively well but underestimates the gap size, see Fig. 2(c). As  $|E_z|$  increases, the gap becomes narrower, and it closes at  $E_z = \eta s E_{z,c}$ , where germanene becomes semimetallic. As  $|E_z|$  increases further, the gap opens again. Reduction of the field back to  $E_{z,c}$  closes the trivial gap and germanene becomes again a semimetal. This opening and closing of the trivial gap is shown in Fig. 2(d). Note that the magnitude of the electric field may include a systematic error of up to 50% [16], caused by difficulties in estimating the tip-sample distance, work functions, image charges, and tip-induced band bending. Miscalculations of these contributions would simply lead to an offset, and will not affect the qualitative picture, i.e., the linear dependence of the gap size on  $|E_z - E_{z,c}|$ .

We now focus our attention on the effect of the electric field on the edge states. Figure 3(a) provides the differential conductance  $dI(V)/dV$  spectra recorded at a germanene edge for a field of  $E_z = E_{z,c}$ . For comparison, we also provide the corresponding bulk differential conductance. For  $E_z = E_{z,c}$ , the bulk topological gap is closed and germanene is a topological semimetal having a characteristic V-shaped DOS. The metallic edge states remain but are shifted to higher energies, Fig. 3(a), in line with our calculations in Fig. 2(a). Similar to  $E_z < E_{z,c}$ , the edge states have a 1D character, Fig. 3(b), and are still robust to disorder and termination independent, see Fig. S6. For  $E_z > E_{z,c}$ , a trivial gap opens at the bulk of germanene, and the edge states vanish, see Figs. 3(c) and 3(d). The DOS at

the edges is comparable to that of the bulk. Indeed, in line with our TB calculations, Fig. 2(a), at this high field, the topologically protected edge states become trivial and are pushed to the bulk bands of germanene. We mapped the transition of the edge channels in Fig. 3(e) for energies near the two edge states. A reversible switch of the topologically protected channels from *on* at  $E_z \leq E_{z,c}$  to *off* at  $E_z > E_{z,c}$  is fully within experimental reach. As a final remark, we note that while STM-STS has its limitations, it is the only experimental technique that provides the required spatial resolution to scrutinize QSH edge states.

We demonstrated that germanene is a QSH insulator, characterized by a bulk band gap ( $\sim 70$  meV for a field of 1.6 V/nm) and robust metallic edge states. The application of a perpendicular, tip-induced, electric field alters the local DOS of germanene. The topological gap decreases by increasing the strength of the electric field and completely closes at a critical field of  $\sim 1.95$  V/nm. Increasing further the strength of the electric field opens a trivial gap ( $\sim 70$  meV for a field of 2.32 V/nm) and switches the edge states off. The gap size depends linearly on the strength of the electric field. The results are supported by TB and DFT calculations based on the Kane-Mele model. These properties make germanene an excellent candidate for deepening our understanding of topological effects and realizing their potential in topological devices such as a topological field-effect transistor [30,63–66].

P. B., C. C., and H. J. W. Z. acknowledge NWO Veni and NWO Grant No. 16PR3237 for financial support. M. E. acknowledges CREST, JST Grant No. JPMJCR20T2 for financial support. A. N. R. acknowledges the European Research Council via Synergy Grant No. 854843 FASTCORR. Y. L., C.-C. L., and Y. Y. acknowledge the National Key R&D Program of China Grant No. 2020YFA0308800 and the NSF of China Grants No. 11922401 and No. 12061131002. P. B. and H. J. W. Z. would also like to acknowledge Professor J. W. M. Hilgenkamp, Professor Thom Palstra, Dr. G. H. L. A. Brocks, and Dr. P. L. de Boeij for fruitful discussions.

\*p.bampoulis@utwente.nl

- [1] C. L. Kane and E. J. Mele, *Phys. Rev. Lett.* **95**, 226801 (2005).
- [2] C. L. Kane and E. J. Mele, *Phys. Rev. Lett.* **95**, 146802 (2005).
- [3] F. D. M. Haldane, *Phys. Rev. Lett.* **61**, 2015 (1988).
- [4] M. Z. Hasan and C. L. Kane, *Rev. Mod. Phys.* **82**, 3045 (2010).
- [5] B. A. Bernevig, T. L. Hughes, and S.-C. Zhang, *Science* **314**, 1757 (2006).
- [6] B. A. Bernevig and S.-C. Zhang, *Phys. Rev. Lett.* **96**, 106802 (2006).
- [7] C. Wu, B. A. Bernevig, and S.-C. Zhang, *Phys. Rev. Lett.* **96**, 106401 (2006).
- [8] X.-L. Qi and S.-C. Zhang, *Rev. Mod. Phys.* **83**, 1057 (2011).
- [9] M. Konig, S. Wiedmann, C. Brune, A. Roth, H. Buhmann, L. W. Molenkamp, X.-L. Qi, and S.-C. Zhang, *Science* **318**, 766 (2007).
- [10] A. Roth, C. Brüne, H. Buhmann, L. W. Molenkamp, J. Maciejko, X.-L. Qi, and S.-C. Zhang, *Science* **325**, 294 (2009).
- [11] T. Li, P. Wang, H. Fu, L. Du, K. A. Schreiber, X. Mu, X. Liu, G. Sullivan, G. A. Csáthy, X. Lin *et al.*, *Phys. Rev. Lett.* **115**, 136804 (2015).
- [12] I. Knez, R.-R. Du, and G. Sullivan, *Phys. Rev. Lett.* **107**, 136603 (2011).
- [13] S. Wu, V. Fatemi, Q. D. Gibson, K. Watanabe, T. Taniguchi, R. J. Cava, and P. Jarillo-Herrero, *Science* **359**, 76 (2018).
- [14] S. Tang, C. Zhang, D. Wong, Z. Pedramrazi, H.-Z. Tsai, C. Jia, B. Moritz, M. Claassen, H. Ryu, S. Kahn *et al.*, *Nat. Phys.* **13**, 683 (2017).
- [15] Z. Fei, T. Palomaki, S. Wu, W. Zhao, X. Cai, B. Sun, P. Nguyen, J. Finney, X. Xu, and D. H. Cobden, *Nat. Phys.* **13**, 677 (2017).
- [16] J. L. Collins, A. Tadich, W. Wu, L. C. Gomes, J. N. Rodrigues, C. Liu, J. Hellerstedt, H. Ryu, S. Tang, S.-K. Mo *et al.*, *Nature (London)* **564**, 390 (2018).
- [17] Y. Yao, F. Ye, X.-L. Qi, S.-C. Zhang, and Z. Fang, *Phys. Rev. B* **75**, 041401(R) (2007).
- [18] A. Acun, L. Zhang, P. Bampoulis, M. Farmanbar, A. van Houselt, A. N. Rudenko, M. Lingenfelder, G. Brocks, B. Poelsema, M. I. Katsnelson *et al.*, *J. Phys. Condens. Matter* **27**, 443002 (2015).
- [19] L. Zhang, P. Bampoulis, A. N. Rudenko, Q. Yao, A. van Houselt, B. Poelsema, M. I. Katsnelson, and H. J. W. Zandvliet, *Phys. Rev. Lett.* **116**, 256804 (2016).
- [20] P. Bampoulis, L. Zhang, A. v. Safaei, R. van Gastel, B. Poelsema, and H. J. Zandvliet, *J. Phys. Condens. Matter* **26**, 442001 (2014).
- [21] F.-f. Zhu, W.-j. Chen, Y. Xu, C.-l. Gao, D.-d. Guan, C.-h. Liu, D. Qian, S.-C. Zhang, and J.-f. Jia, *Nat. Mater.* **14**, 1020 (2015).
- [22] F. Reis, G. Li, L. Dudy, M. Bauernfeind, S. Glass, W. Hanke, R. Thomale, J. Schäfer, and R. Claessen, *Science* **357**, 287 (2017).
- [23] J. Deng, B. Xia, X. Ma, H. Chen, H. Shan, X. Zhai, B. Li, A. Zhao, Y. Xu, W. Duan *et al.*, *Nat. Mater.* **17**, 1081 (2018).
- [24] F. Matusalem, M. Marques, L. K. Teles, L. Matthes, J. Furthmüller, and F. Bechstedt, *Phys. Rev. B* **100**, 245430 (2019).
- [25] N. R. Glavin, R. Rao, V. Varshney, E. Bianco, A. Apte, A. Roy, E. Ringe, and P. M. Ajayan, *Adv. Mater.* **32**, 1904302 (2020).
- [26] F. Bechstedt, P. Gori, and O. Pulci, *Prog. Surf. Sci.* **96**, 100615 (2021).
- [27] C.-C. Liu, W. Feng, and Y. Yao, *Phys. Rev. Lett.* **107**, 076802 (2011).
- [28] S. Cahangirov, M. Topsakal, E. Aktürk, H. Şahin, and S. Ciraci, *Phys. Rev. Lett.* **102**, 236804 (2009).
- [29] M. Ezawa, *New J. Phys.* **14**, 033003 (2012).
- [30] X. Qian, J. Liu, L. Fu, and J. Li, *Science* **346**, 1344 (2014).
- [31] L. Matthes and F. Bechstedt, *Phys. Rev. B* **90**, 165431 (2014).
- [32] M. Ezawa, *J. Phys. Soc. Jpn.* **84**, 121003 (2015).

- [33] W. G. Vandenberghe and M. V. Fischetti, *Nat. Commun.* **8**, 14184 (2017).
- [34] See Supplemental Material at <http://link.aps.org/supplemental/10.1103/PhysRevLett.130.196401> for Germanene growth: spinodal decomposition, Scanning tunneling microscopy, Preparation of metal coated tips, Tight-binding model of germanene, Dirac theory of germanene, DOS and conductance, DFT calculations, Germanene coupling to the substrate, Determination of the band gap, Edge states, Proximity effects, Built-in electric field, and Tip-induced band bending, which includes Refs. [35–54].
- [35] P. Bampoulis, A. Acun, L. Zhang, and H. J. Zandvliet, *Surf. Sci.* **626**, 1 (2014).
- [36] R. van Bremen, P. Bampoulis, J. Aprojanz, M. Smithers, B. Poelsema, C. Tegenkamp, and H. J. Zandvliet, *J. Appl. Phys.* **124**, 125301 (2018).
- [37] M. Will, P. Bampoulis, T. Hartl, P. Valerius, and T. Michely, *ACS Appl. Mater. Interfaces* **11**, 40524 (2019).
- [38] C.-C. Liu, H. Jiang, and Y. Yao, *Phys. Rev. B* **84**, 195430 (2011).
- [39] S. Datta, *Electronic Transport in Mesoscopic Systems* (Cambridge University Press, Cambridge, 1995); *Quantum Transport: Atom to Transistor* (Cambridge University Press, England, 2005).
- [40] M. L. Sancho, J. L. Sancho, J. L. Sancho, and J. Rubio, *J. Phys. F* **15**, 851 (1985).
- [41] F. Muñoz-Rojas, D. Jacob, J. Fernández-Rossier, and J. Palacios, *Phys. Rev. B* **74**, 195417 (2006).
- [42] D. A. Areshkin and B. K. Nikolić, *Phys. Rev. B* **79**, 205430 (2009).
- [43] L. P. Zárbo and B. Nikolić, *Europhys. Lett.* **80**, 47001 (2007).
- [44] T. Li and S.-P. Lu, *Phys. Rev. B* **77**, 085408 (2008).
- [45] M. Ezawa, *Appl. Phys. Lett.* **102**, 172103 (2013).
- [46] J. P. Perdew, K. Burke, and M. Ernzerhof, *Phys. Rev. Lett.* **77**, 3865 (1996).
- [47] G. Kresse and J. Furthmüller, *Phys. Rev. B* **54**, 11169 (1996).
- [48] L. Zhang, P. Bampoulis, A. van Houselt, and H. J. Zandvliet, *Appl. Phys. Lett.* **107**, 111605 (2015).
- [49] K. Nakada, M. Fujita, G. Dresselhaus, and M. S. Dresselhaus, *Phys. Rev. B* **54**, 17954 (1996).
- [50] P. Koskinen, S. Malola, and H. Häkkinen, *Phys. Rev. Lett.* **101**, 115502 (2008).
- [51] S. K. Hämäläinen, Z. Sun, M. P. Boneschanscher, A. Uppstu, M. Ijäs, A. Harju, D. Vanmaekelbergh, and P. Liljeroth, *Phys. Rev. Lett.* **107**, 236803 (2011).
- [52] L. Liang, J. Wang, W. Lin, B. G. Sumpter, V. Meunier, and M. Pan, *Nano Lett.* **14**, 6400 (2014).
- [53] Y. Tison, J. Lagoute, V. Repain, C. Chacon, Y. Girard, F. Joucken, R. Sporken, F. Gargiulo, O. V. Yazyev, and S. Rousset, *Nano Lett.* **14**, 6382 (2014).
- [54] I. Battisti, V. Fedoseev, K. M. Bastiaans, A. De La Torre, R. S. Perry, F. Baumberger, and M. P. Allan, *Phys. Rev. B* **95**, 235141 (2017).
- [55] C. Huang, J. Zhou, H. Wu, K. Deng, P. Jena, and E. Kan, *J. Phys. Chem. Lett.* **7**, 1919 (2016).
- [56] A. Popescu, P. Rodriguez-Lopez, and L. M. Woods, *Phys. Rev. Mater.* **3**, 064002 (2019).
- [57] A. Avsar, J. Y. Tan, T. Taychatanapat, J. Balakrishnan, G. Koon, Y. Yeo, J. Lahiri, A. Carvalho, A. Rodin, E. O'Farrell *et al.*, *Nat. Commun.* **5**, 4875 (2014).
- [58] A. López, L. Colmenárez, M. Peralta, F. Mireles, and E. Medina, *Phys. Rev. B* **99**, 085411 (2019).
- [59] C. Pauly, B. Rasche, K. Koepernik, M. Liebmann, M. Pratzer, M. Richter, J. Kellner, M. Eschbach, B. Kaufmann, L. Plucinski *et al.*, *Nat. Phys.* **11**, 338 (2015).
- [60] Y. Shi, J. Kahn, B. Niu, Z. Fei, B. Sun, X. Cai, B. A. Francisco, D. Wu, Z.-X. Shen, X. Xu *et al.*, *Sci. Adv.* **5**, eaat8799 (2019).
- [61] N. D. Drummond, V. Zolyomi, and V. I. Fal'ko, *Phys. Rev. B* **85**, 075423 (2012).
- [62] B. Borca, C. Castenmiller, M. Tsvetanova, K. Sothewes, A. N. Rudenko, and H. J. Zandvliet, *2D Mater.* **7**, 035021 (2020).
- [63] A. Molle, J. Goldberger, M. Houssa, Y. Xu, S.-C. Zhang, and D. Akinwande, *Nat. Mater.* **16**, 163 (2017).
- [64] Y. Ren, Z. Qiao, and Q. Niu, *Rep. Prog. Phys.* **79**, 066501 (2016).
- [65] W. Han, Y. Otani, and S. Maekawa, *npj Quantum Mater.* **3**, 27 (2018).
- [66] M. S. Lodge, S. A. Yang, S. Mukherjee, and B. Weber, *Adv. Mater.* **33**, 2008029 (2021).